Statistical Shape and Appearance Model of Left Atrial Geometry and Conduction Velocity in Atrial Fibrillation

Alexander J Sharp[1,2], Timothy R Betts[2], Abhirup Banerjee[1]

[1]Department of Engineering Science, University of Oxford, Oxford, UK
[2]Department of Cardiology, Oxford University Hospitals NHS Foundation Trust, Oxford, UK

Abstract

Synthetic atria are increasingly used in in silico studies of atrial fibrillation (AF). However, existing models frequently rely on randomly assigned fibrosis maps, capturing only one facet of arrhythmogenicity and neglecting the interplay between geometry and other elements of negative remodelling that define atrial cardiomyopathy. We propose a novel statistical shape and appearance model (SSAM) of the left atrium, using charge density mapping data from 49 patients with persistent AF. Our findings show that local anatomical features correlate with CV. By jointly modelling shape and CV, our SSAM has the potential of generating synthetic atria that encode the coupled remodelling processes characteristic of AF, enabling large-scale in silico investigations.

1. Introduction

In silico studies of AF are increasingly being used to understand arrhythmia mechanisms and assess therapies. However, generating realistic and functionally meaningful synthetic atria remains a major challenge.

Synthetic patient approaches benefit from the relative ease of generating large datasets, for example for machine learning applications, avoiding the time-consuming segmentation of individual images required when using real patients [1]. Statistical shape models (SSMs) are a powerful approach to capture anatomical variability across patient populations and have been successfully applied in the generation of realistic atrial geometries [1]. In the context of AF, fibrosis has subsequently been used to inform the arrhythmogenic substrate, assigning random or probabilistically guided fibrosis patterns to the generated geometries [2,3].

However, this method has key limitations. Firstly, not all AF patients exhibit significant fibrotic remodelling, with 64% of patients in the ERASE-AF study having no low voltage areas [4]. Secondly, it models fibrosis independently of atrial geometry, despite both being components of the negative remodelling that defines atrial cardiomyopathy [5]. There is evidence they are interconnected, with left atrial diameter differing significantly between groups stratified by the extent of low-voltage areas in a cohort of ~1,500 patients [6]. Ignoring this relationship may lead to the creation of non-physiological synthetic atria, thus compromising the validity of findings from *in silico* studies.

Unlike fibrosis, conduction velocity (CV) implicitly reflects multiple underlying structural and functional mechanisms of arrhythmogenesis, including tissue anisotropy, interstitial fibrosis, and ion channel remodelling [7]. It is known to influence re-entry dynamics, and is linked to AF burden, disease progression, and recurrence post-pulmonary vein (PV) isolation [8]. Yet CV mapping requires invasive intracardiac catheterisation, limiting its availability to specialised centres and a small subset of patients. This poses a major barrier to generating large populations of real patients.

In this study, we aimed to develop a statistical shape and appearance model (SSAM) of the left atrium (LA) that integrates real-world CV data, providing a powerful tool for generating synthetic atria. By capturing the interconnected nature of anatomical and functional remodelling in AF, and by using CV as a more nuanced determinant of the AF substrate, our SSAM has the potential to improve the physiological fidelity of large-scale *in silico* studies of AF.

2. Methods

2.1. Data Acquisition

Data were obtained from 49 patients with persistent AF enrolled in the DISCOVER registry (NCT03893331). Patient characteristics are summarised in Table 1.

All patients underwent first-time catheter ablation guided by charge density mapping using the AcQMap system (Acutus Medical, CA, USA) [8]. A 20-second recording of either presenting or induced AF, acquired prior to any ablation, was used to compute CV at each mesh vertex across multiple wavefronts, with the median value per vertex retained.

Table 1. Patient characteristics.

Characteristics	Distribution
Age, years, mean ± SD	61 ± 12
Sex, *n* (%)	
Male	43 (80)
Female	11 (20)
BMI (kg/m^2), mean ± SD	30 ± 5
CHA_2DS_2-VASc score, median (IQR)	1.5 (0 – 3)
Time from AF diagnosis, months, median (IQR)	29 (15 – 38)
AF mapped, *n* (%)	
Spontaneous	41 (76)
Induced	13 (24)

2.2. SSM

LA anatomies were reconstructed using intra-chamber ultrasound. These geometries have previously been shown to compare favourably with magnetic resonance imaging [9]. PVs and the mitral valve were excluded to standardise anatomy. Meshes were downsampled to 4,500 vertices and processed using the particle-based shape modelling workflow in ShapeWorks 6.4 [10]. A set of 576 correspondences was computed per subject, and their 3D coordinates exported for further analysis in MATLAB R2022b (MathWorks, MA, USA). Principal Component Analysis (PCA) was applied to the concatenated coordinates to extract modes of anatomical variation.

2.3. Statistical Appearance Model (SAM)

CV values were assigned to each correspondence using a nearest neighbour algorithm based on the nearest mesh vertex, generating a CV appearance vector per subject $[a_1, a_2, \dots, a_{576}]$. PCA was applied to these vectors to identify dominant patterns in CV distribution. Spearman correlations between shape and CV modes were computed to assess structure-function relationships.

2.4. SSAM

To integrate anatomical and functional variability, an SSAM was constructed. Each subject was represented by a combined vector: $[x_1, y_1, z_1, a_1, \dots, x_{576}, y_{576}, z_{576}, a_{576}]$. Prior to PCA, CV values were normalised using the IQR to ensure comparability with spatial coordinates. Subsequently, PCA modes captured the joint variation in shape and CV.

For each mode i, the relative contributions of shape and CV were quantified as:

- $Shape\ contribution\ (PC_i) = \frac{\sum |shape\ loadings|}{\sum |all\ loadings|}$
- $CV\ contribution\ (PC_i) = \frac{\sum |CV\ loadings|}{\sum |all\ loadings|}$

3. Results

3.1. Model Variance Explanation

Figure 1 shows cumulative variance by mode for each model. To reach 95% variance, 20, 22, and 27 modes were needed for our SSM, SAM, and SSAM, respectively. Explained variance for each mode is depicted in Figures 2 (SSM and SAM) and 3 (SSAM).

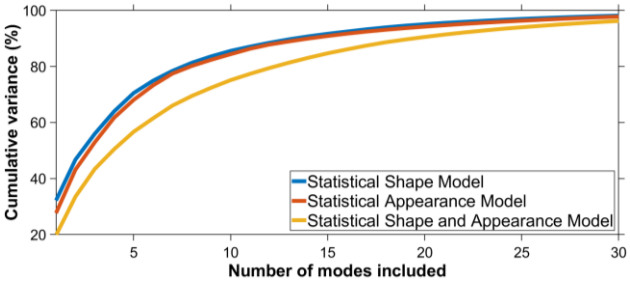

Figure 1. Cumulative variance covered for different numbers of modes for all models.

SSM mode 1 primarily captured LA volume. Subsequent modes (2, 3, and 4) represented different combinations of atrial width, anteroposterior (AP) diameter, and varying degrees of posterior wall protrusion or concavity.

SAM mode 1 represented global CV, with subsequent modes highlighting spatial patterns, such as anterior–posterior differences and PV ostial conduction.

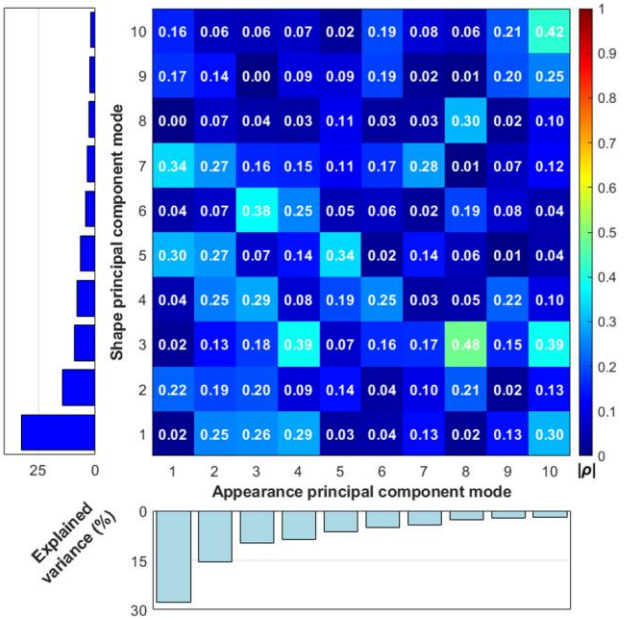

Figure 2. Correlation matrix between shape and appearance modes (main plot). Explained variance for individual shape and appearance modes are shown in the left and bottom subplots, respectively.

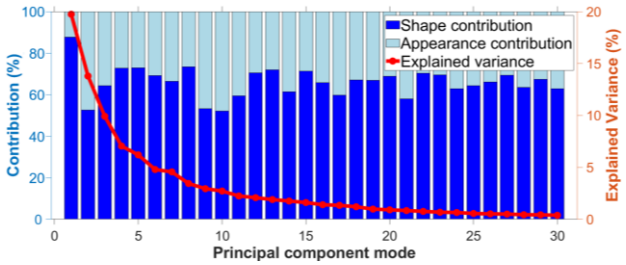

Figure 3. Relative contributions of shape and CV to statistical shape and appearance model modes (blue). Explained variance for individual modes (red).

3.2. Relationship Between Shape and CV

Shape mode 3 showed a moderate correlation with appearance mode 8 ($\rho = 0.48$; Figure 2). This combination was characterised by reduced CV on the posterior wall, especially near the left inferior PV, when the posterior wall was more concave, and reduced inferior wall and roof CV with a smaller AP diameter (Figure 4). Several other weaker correlations between shape and appearance modes were also observed.

3.3. SSAM

Figure 3 illustrates the relative contributions of shape and CV to each SSAM mode, while Figure 5 visualises variation along the first four modes.

Mode 1 was shape-dominant, mirroring SSM Mode 1 (LA volume). Larger atria tended to exhibit slower CV, particularly on the anterior wall. Mode 2 was equal parts CV and shape-driven, reflecting global CV slowing (similar to SAM mode 1), in larger atria with a less prominent left atrial appendage. Modes 3 and 4 captured the interplay between shape and CV seen in earlier analyses, recapitulating associations such as a concave posterior wall with slower local CV, and reduced AP diameter with slower conduction on the inferior wall.

4. Discussion and Conclusion

In this study, we developed and analysed an SSAM of the LA that integrates anatomical and CV variability in persistent AF. Our results highlight the interdependence of structural and functional remodelling, demonstrating that combining shape and CV data offers deeper insight into AF substrate heterogeneity than analysing either alone.

4.1. Key Anatomical Features and AF Dynamics

As expected, larger LA volumes were associated with a greater spatial extent of slow CV. However, our novel, spatially resolved analyses also revealed that local shape features influenced CV distribution.

Increased concavity, in regions such as the posterior wall, corresponded with locally reduced CV. Mechanistically, this may reflect geometric constraints or external compression from adjacent structures, potentially promoting tissue remodelling [11,12]. Additionally, local curvature could alter fibre orientation or myocardial thickness, influencing CV.

4.2. Utility of SSAM for Virtual Populations

A key motivation for this work is the growing demand for synthetic, yet physiologically informed, virtual patient populations. By jointly modelling shape and CV as modes of variation, our SSAM enables the generation of synthetic LA that more faithfully capture the coupled structural and functional remodelling characteristic of AF. This feature addresses a central limitation in existing synthetic models, which frequently impose fibrosis patterns without considering their anatomical context. Moreover, CV may be a more sensitive indicator of arrhythmogenic substrate than fibrosis alone.

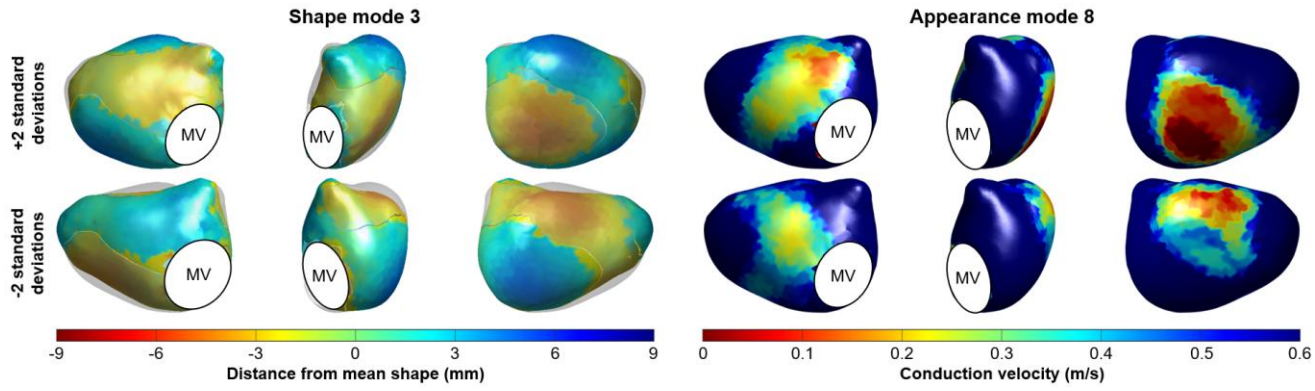

Figure 4. Variation in modes, showing ±2 standard deviations from the mean. Left: shape mode 3, with distance from mean shape (light grey); right: appearance mode 8, with conduction velocity distributions depicted on mean shape. MV: mitral valve.

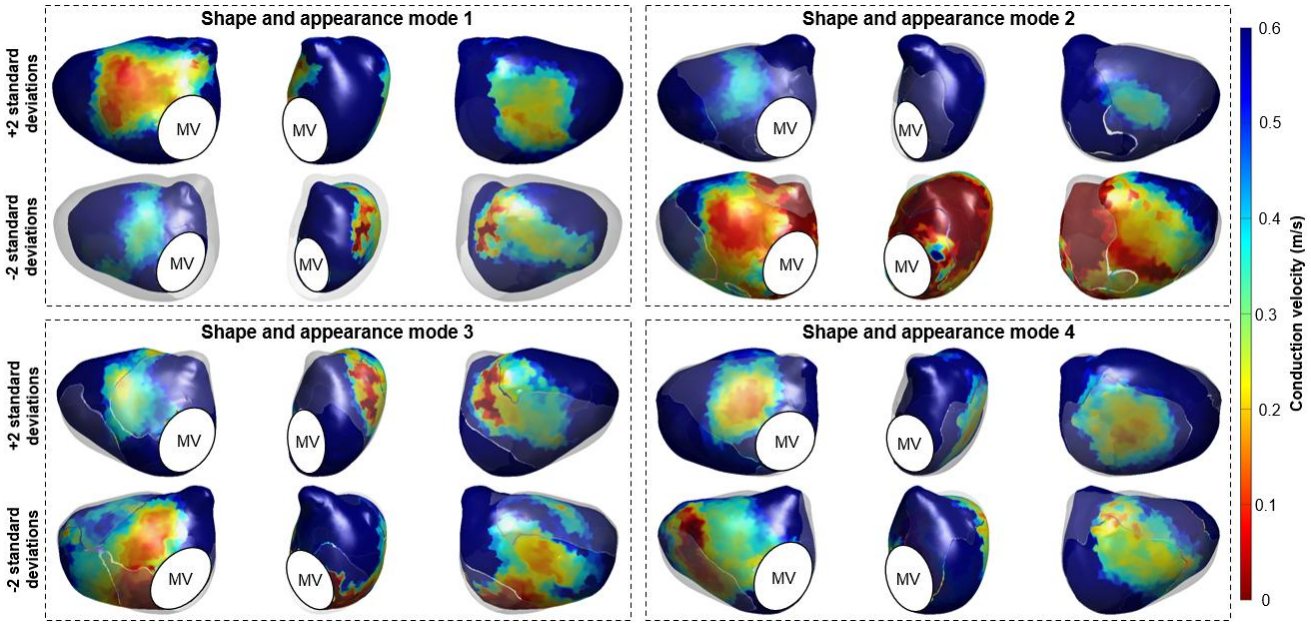

Figure 5. Variation in first 4 Statistical Shape and Appearance Model modes, showing ±2 standard deviations from the mean. MV: mitral valve.

Acknowledgments

This work was supported by a Heart Research UK Novel and Emerging Technologies Grant (NET25-100009). AB is supported by a Royal Society University Research Fellowship (URF\R1\221314). We thank the DISCOVER investigators and centres for their data contributions.

References

[1] C. Nagel, S. Schuler, O. Dössel, and A. Loewe, "A bi-atrial statistical shape model for large-scale in silico studies of human atria: Model development and application to ECG simulations," *Medical Image Analysis*, vol. 74, pp. 102210, Dec. 2021.

[2] A. Dasí et al., "In Silico TRials guide optimal stratification of ATrIal FIbrillation patients to Catheter Ablation and pharmacological medicaTION: the i-STRATIFICATION study," *Europace*, vol. 26, no. 6, pp. euae150, Jun. 2024.

[3] A. M. Zolotarev et al., "Predicting atrial fibrillation treatment outcome with siamese multi-modal fusion and cardiac digital twins," *Proceedings of the Medical Imaging with Deep Learning*, 2024

[4] Y. Huo et al., "Low-voltage myocardium-guided ablation trial of persistent atrial fibrillation," *NEJM Evidence*, vol. 1, no. 11, pp. EVIDoa2200141, Oct. 2022.

[5] A. J. Sharp, T. R. Betts, A. Banerjee, "Leveraging 3D atrial geometry for the evaluation of atrial fibrillation: a comprehensive review," *Journal of Clinical Medicine*, vol. 13, no. 15, pp. 4442, Jul. 2024.

[6] M. Masuda et al., "Prognostic impact of atrial cardiomyopathy: long-term follow-up of patients with and without low-voltage areas following atrial fibrillation ablation," *Heart Rhythm*, vol. 21, no. 4, pp. 378–386, Apr. 2024.

[7] S. Coveney, C. Cantwell, and C. Roney, "Atrial conduction velocity mapping: clinical tools, algorithms and approaches for understanding the arrhythmogenic substrate," *Medical & Biological Engineering & Computing*, vol. 60, no. 9, pp 2463-2478, Sep. 2022.

[8] A. J. Sharp et al., "Identifying extra pulmonary vein targets for persistent atrial fibrillation ablation: bridging advanced and conventional mapping techniques," *Europace*, vol. 27, no. 4, pp. euaf048, Mar. 2025.

[9] A. J. Sharp et al., "Multi-modal integration of MRI and global chamber charge density mapping for the evaluation of atrial fibrillation," *Royal Society Open Science*, vol. 12, no. 1, pp. 241048, Jan. 2025.

[10] J. Cates, S. Elhabian, and R. Whitaker, "Shapeworks: particle-based shape correspondence and visualization software," in *Statistical Shape and Deformation Analysis*, 2017, pp. 257–298.

[11] G. Caixal et al., "Proximity to the descending aorta predicts regional fibrosis in the adjacent left atrial wall: Aetiopathogenic and prognostic implications," *Europace*, vol. 23, no. 10, pp. 1559–1567, Oct. 2021.

[12] S. Hayashida et al., "Formation of low-voltage zones on the anterior left atrial wall due to mechanical compression by the ascending aorta," *Journal of Cardiovascular Electrophysiology*, vol. 32, no. 8, pp. 2275–2284, Aug. 2021.

Address for correspondence:

Alexander James Sharp
Institute of Biomedical Engineering, Old Road Campus Research Building, Oxford, OX3 7DQ, United Kingdom
alexander.sharp@eng.ox.ac.uk